applied sciences

MDPI

Review

Review and Perspectives of Aurivillius Structures as a Lead-Free Piezoelectric System

Alberto Moure

Instituto de Cerámica y Vidrio, CSS Group (Electroceramic Department), Consejo Superior de Investigaciones Científicas (CSIC), C/Kelsen, 5 28049 Madrid, Spain; alberto.moure@icv.csic.es;
Tel: +34-917-355-840; Fax: +34-917-355-843

Received: 2 October 2017; Accepted: 30 November 2017; Published: 3 January 2018

Abstract: According to the EU-Directives 2002/95/EC, 2002/96/EC, lead-based piezoceramics must be substituted in the future with more environmentally friendly alternatives, only when a reliable alternative is found. This is why an increasing interest has grown in the research community to find lead free piezoelectric materials that fulfil the requirements for this substitution. Different families of compounds have been shown to be possible candidates for this use, such as bismuth and niobates based perovskites, pyrochlores, etc. However, a material with piezoelectric coefficients similar to those of PZT (lead zirconate titanate, $Pb[Zr_xTi_{1-x}]O_3$) has not been yet found. Besides, each of these families has its specific characteristics in terms of remnant polarization, coercive field or application temperature. Thus, the choice of each material should be made according to the specific needs of the application. In this sense, Aurivillius-type structure materials (also known as Bismuth Layered Structure Ferroelectrics, BLSF) can take advantage of their specific properties for uses as Lead Free Piezoelectric systems. Some of them have a high Curie temperature, which make them good candidates to be used as high temperature piezoelectrics; high coercive fields, which facilitates their use as actuators; or a high switching fatigue resistance, which can be useful for future applications as Ferroelectric Random Access Memories (FERAM).

Keywords: bismuth layered ferroelectric structures; aurivillius; piezoelectric; multiferroic

1. Overview

Many of the peculiar characteristic properties of Aurivillius materials are determined by their crystalline structure. These compounds have the general formula $[Bi_2O_2]^{2+}[A_{n-1}B_nO_{3n+1}]^{2-}$ and are built from n pseudoperovskite layers alternating with $[Bi_2O_2]^{2+}$ layers [1]. Figure 1 shows the prototype of the Aurivillius structure as a function of the number of pseudo-perovskite layers [2]. The "n" values can range from 1 to ∞. In this case (n = ∞), the repeated cell is the pure perovskite. The number of perovskites can be odd, even or a mixture. Examples of each case are Bi_2WO_6 (n = 1) and $Bi_4Ti_3O_{12}$ (n = 3); Bi_3TiNbO_9, $SrBi_2Nb_2O_9$ (n = 2) and $CaBi_4Ti_4O_{12}$ (n = 4); an example for a mixture Aurivillius is $Bi_7Ti_4NbO_{21}$. In this case, layers with 2 or 3 pseudo-perovskites are alternated with the $[Bi_2O_2]^{2+}$ layers.

At difference of the ferroelectrics with perovskite structure, the polarization is not produced by the displacement of the B cation within the oxygen octahedral but by relative shifts of the oxygen octahedral through the a-axis with respect to the [001] bismuth chain. They can be divided in 3 main movements, as illustrated in references [3–5]:

- Oxygen octahedral in the a-axis.
- Relative displacements in the opposite direction to B cations of the perovskite with respect to the octahedral.
- Displacement through the a-axis of the oxygen ions of the Bi-O layer.

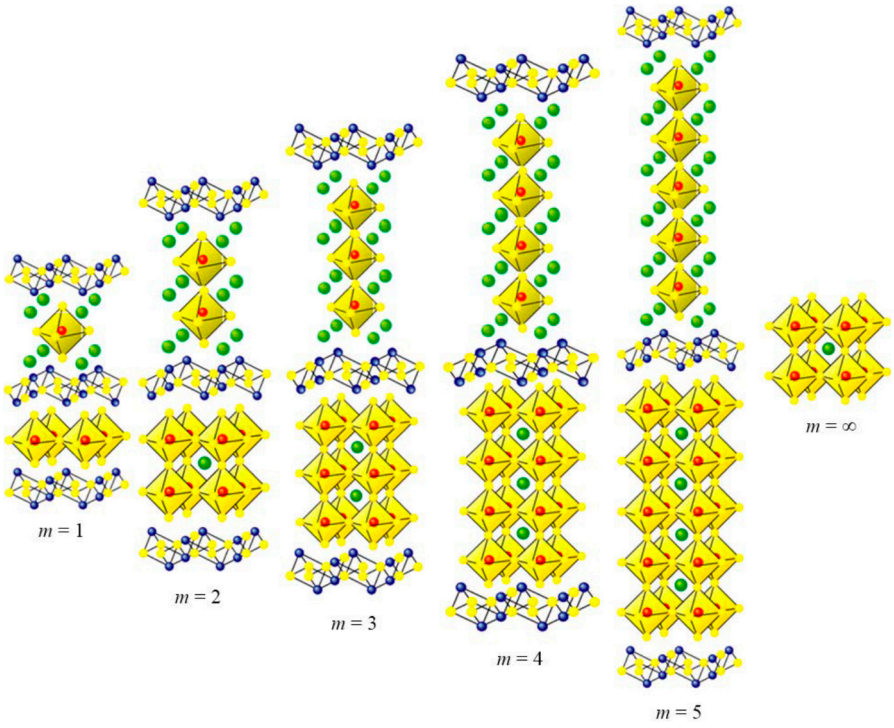

Figure 1. Prototype of the Aurivillius structure as a function of the number of pseudo-perovskite layers (taken from [2]).

Besides, this particular crystalline structure determines the growth habit for these materials. They grow with anisotropic shapes, as platelets with the minor dimension in parallel to the c-axis. This is a disadvantage for the sintering process to obtain dense bulk ceramics but it favors the grain alignment that allows the texture and the crystal orientation. It can be carried out by different means, as hot pressing, tape-casting, templated grain growth or others, as will be explained in Section 2.1.

2. Processing of Ceramics with Aurivillius Type Structure

Ceramic method is the most used route for the processing of the ceramics with Aurivillius type structure. It is ideal because of its low cost and the possibility of obtaining high amounts of material. The synthesis is carried out by calcination at relatively high temperatures of precursors containing the structure components, mainly oxides and carbonates. The ceramics are usually obtained by sintering in air of pressed green pellets. A major drawback for this method is to have dense ceramics with adequate grain size. Its lamellar crystal growth makes the compaction of the precursor ceramic powder more difficult and the reduced mass transport during sintering leads to porous ceramics (higher than 10% of porosity) [6], which makes difficult their uses in piezoelectric applications.

An approach to solve this problem is to use alternative synthesis methods to obtain precursors with a homogenous particle distribution characterized by small sizes and isotropic shapes. It will provide a better packing of the green pellet and a higher reactivity that allows the reduction of the processing temperature. Some of these alternative methods are detailed in the following sections.

(a) *Hydrothermal synthesis*. In this technique, the combination of temperature and high pressure produced by water solutions in an autoclave allows the synthesis of materials with special characteristics in terms of small grain sizes (even in the nanometer scale) and particular and controlled shapes. The application to Aurivillius structure materials synthesis has been deeply explored in several works. Depending on variables such as time or temperature (<300 °C) [7], use of different mineralizers and concentrations [8] or starting materials [9], single phase materials with different sizes and shapes from the nanometric to micrometric scale can be synthesized.

They give place to ceramics with relatively high densities, as shown in Figure 2 [10] with good ferro/piezoelectric properties [7,11].

(b) *Sol-gel*. In this process, the solution evolves gradually through hydrolysis and polycondensation reactions towards the formation of a gel-like network to form a colloid. The mixture at practically atomic level favors the reaction to synthesize precursors at low temperatures, allowing the control of particle size and shape. Thus, different compositions with Aurivillius-type structure were synthesized, at temperatures that can range from 525 to 700 °C [12–16] to have particles in the nanometric scale, as shown in Figure 3. Dense ceramics with high remnant polarization (24.15 $\mu C/cm^2$) values can be achieved by this route in $Bi_4Ti_3O_{12}$ based ceramics [17].

(c) *Coprecipitation*. This is a synthesis route from a solution, in which the addition of a precipitant agent or the solvent evaporation reduces the solubility of the precursors, causing their precipitation. It allows a mixture of the components at low scale, favoring their reactivity in the calcination steps. Single phase materials are obtained at temperatures ranging from 700–800 °C, to have particles with sizes at the nanometric scale [18–21]. Ceramics with high densities (>97%) can be accomplished at low temperature (875 °C) by sintering ceramic precursors obtained by this route [18].

(d) *Mechanochemical activation/mechanosynthesis*. High energy milling produces synthesis reactions (mechanosynthesis) or changes in the size and reactivity of the precursors (mechanochemical activation) that allow the reduction of the processing temperatures. It is accomplished by the high number of defects produced by the milling. Some Aurivillius compositions have been mechanosynthesized, mainly in planetary mills. Thus, $Bi_4Ti_3O_{12}$ has been obtained after 15 h of milling [22], $CaBi_4Ti_4O_{15}$ after 30 h [23], or $SrBi_4Ti_4O_{15}$ after 20 h [24]. In other cases, the synthesis temperature is decreased by obtaining an amorphous powder after milling [25–27]. The high reactivity of the precursors allows sintering of ceramics with low porosity at relatively low temperatures. A further increase in density can be achieved by hot pressing or by processes of recrystallization after hot pressing [28] that allows the control of the microstructure and texture (Figure 5).

(e) *Molten salt synthesis*. It is based on the use of a molten salt mixed to the starting oxide/carbonates precursors to favor the dissolution-precipitation processes assisted by liquid phases. Final products are obtained at lower temperatures than by the classical ceramic route. The most commonly used salts are NaCl, KCl, Na_2SO_4, K_2SO_4 and a mixture of them at eutectic points that reduce the melting temperature. Depending on the used flux and the precursors, the synthesis conditions can vary. Thus, mixing salts with precursors obtained by hydrolysis or coprecipitation, instead of oxides and carbonates, $Bi_4Ti_3O_{12}$ and Bi_3TiNbO_9 can be obtained at 600 and 700 °C, respectively [29,30]. When oxides and carbonates are used, higher temperatures (800–1100 °C) are usually needed to synthesize Aurivillius-type powders with different compositions [31–33]. These high temperatures favor the growth of large plate-like particles that facilitates the processing of textured ceramics as will be explained later. The use of eutectic KCl/NaCl mixtures allows the reduction of synthesis temperatures (800 °C–2 h) [34] leading to small particles as the ones observed in Figure 4 that improve the $Bi_4Ti_3O_{12}$ photocatalytic activities.

(f) *Microwave assisted synthesis*. With the application of microwaves at high frequency, the associated electromagnetic fields will heat materials with high dielectric losses. Alternatively, the heating of susceptors with high microwave absorption can be achieved. The main characteristic for this process is the high heating rate and short times that inhibit grain growth. The synthesis of $BiGdWO_6$, $BiYWO_6$ or $Bi_4Ti_3O_{12}$ in only 10 min has been reported [35,36]. Temperatures of 900–1100 °C have been measured in those articles. This technique is also used in combination with other routes previously described, as molten salts or hydrothermal [37,38] to further improve the synthesis of Aurivillius precursors.

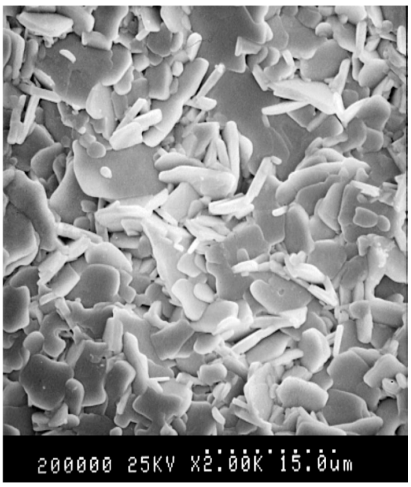

Figure 2. SEM photograph of $Bi_4Ti_3O_{12}$ pellets sintered at 900 °C from hydrothermal synthesized precursor. (Taken from [10]).

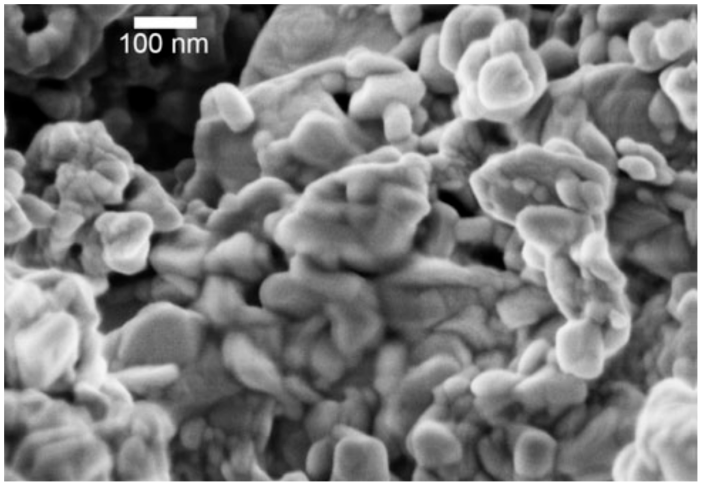

Figure 3. SEM image of nanometric particles of $Bi_2Sr_2TiNb_2O_{12}$ prepared by sol-gel (taken from [14]).

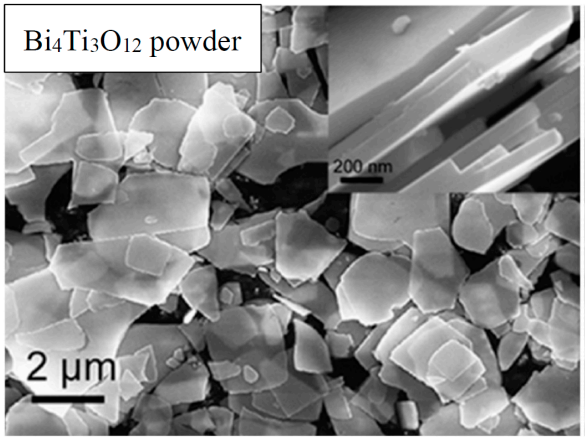

Figure 4. SEM micrographs of $Bi_4Ti_3O_{12}$ powder prepared by the molten salt synthesis method at 800 °C (taken from [34]).

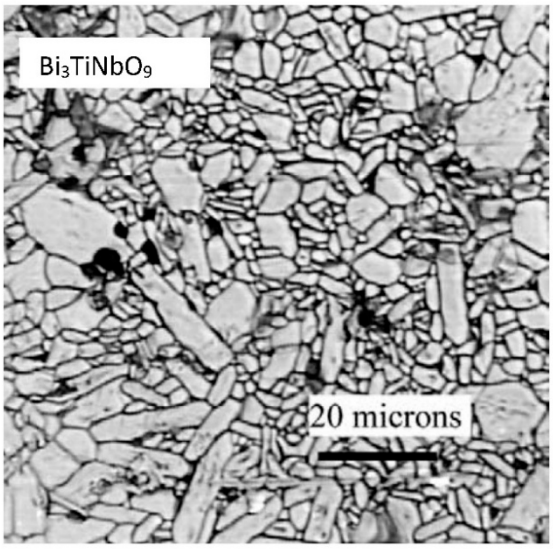

Figure 5. Optical micrographs of polished and thermally etched surfaces of a ceramic are hot-pressed at 900 °C–1 h and correspondingly recrystallized at 1100 °C–1 h (taken from [28]).

2.1. Texture

Another alternative to have dense ceramics with Aurivillius structure is to synthesize the precursors by the classical ceramic or an alternative method and then prepare the ceramics by pressure-assisted sintering. There are three main routes for this: hot-forging, hot pressing and spark plasma sintering. A common characteristic for all these routes is that a relatively high pressure (typically in the order of MPa) is supplied to the green samples at high temperatures, in such way that the thermal and mechanical energy applied favors the closure of porosity.

In the hot-forging technique, a uniaxial pressure is applied to a sample without lateral restrictions [39]. It was one of the first alternative techniques that were used to process highly dense ceramics with bismuth layered structure. Densities higher than 97% are achieved by this method.

A difference between hot-forging and hot pressing is that in this late method, the lateral restriction limits the expansion of the ceramics during sintering [40]. Highly dense ceramics (>99%) at low temperatures can be achieved [41,42]. Spark Plasma Sintering also provides a combination of thermal and mechanical energy for sintering. The main difference with hot-pressing and hot-forging is that heating is produced by pulsed electrical currents that heat the material (or alternatively the graphite die used) due to Joule effect [43]. As examples, densities higher than 95% have been obtained for $CaBi_2Nb_2O_9$ and $Bi_4Ti_3O_{12}$ compositions by SPS, with grain sizes depending on the initial precursors and SPS conditions in terms of temperature (1000–1150 °C) and time [44,45] (Figure 6).

A common characteristic to these methods is that the pressure aligns the platelets grains with the largest faces in perpendicular to the applied pressure (meaning c-axis orientation in parallel to the applied pressure). This gives ceramics with a high level of (00l) texture and thus with anisotropic properties. As the ferroelectric direction lies in the a-b plane in these materials, the samples measured in perpendicular to the pressure will have an enhancement of the ferro-piezoelectric properties with respect to the other direction and to the traditionally isotropic sintered ceramics. As examples, the remnant polarization values are 37, 9.3 and 3.3 $\mu C/cm^2$ for the samples in the perpendicular, parallel direction and for ordinary sintering without pressure, respectively, in hot forged $Bi_4Ti_3O_{12}$ [39]. Bi_3TiNbO_9 ceramics prepared by hot-pressing have d_{33} coefficients: 14–15, 3–4 and 7 pC/N for perpendicular, parallel and ordinary fired samples [46]. In $CaBi_2Nb_2O_9$ ceramics prepared by SPS (Figure 6), these values are 19.5, 0.2 and 7.5 pC/N [44].

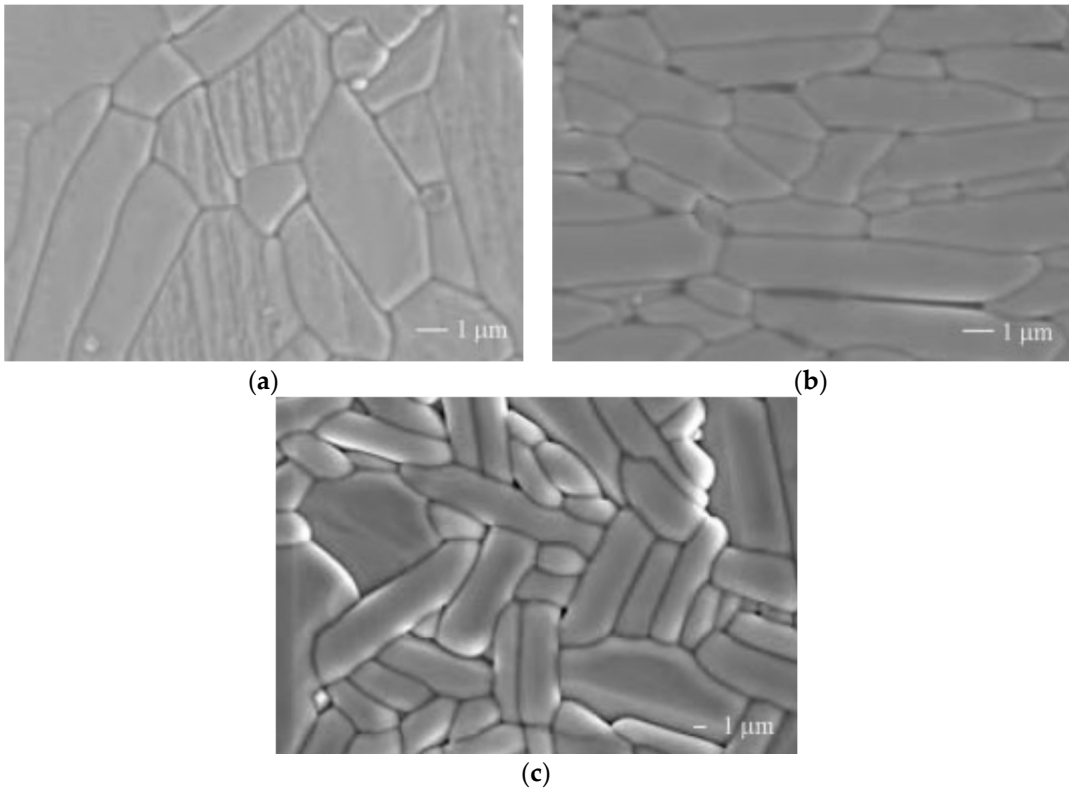

Figure 6. SEM images of polished and thermally etched surfaces for (**a**) perpendicular; (**b**) parallel to the SPS pressing direction; (**c**) conventionally Sintered $CaBi_2Nb_2O_9$ (taken from [44]).

The first experiments leading to the Aurivillus textured ceramic were carried out at the end of the 1970s and the 1980s (with methods still in use today) based on the simultaneous application of high temperature and pressures and were improved by other techniques. Very good results are given by the (reactive) template grain growth after alignment of the anisometric particles by different methods, mainly tape casting or extrusion based molding [47,48]. In the process, large platelet-like particles are aligned in a matrix of powder with the target composition. During the sintering, densification and grain growth with a (00l) preferred orientation occurs. The Lotgering factor is often used to characterize the level of orientation achieved. A value of 0 denotes a random material, while a value of 1 denotes a perfect (00l) orientation. One of the first works that applied this technique for Aurivillius materials was reported by Horn et al. [49]. They proved that only with a 5% of template particles, high densities (97%) and Lotgering factors (~0.96) were obtained by sintering at temperatures higher than 1000 °C. The anisotropy of grain-boundary energies drives grain growth in BiT and the grain rotation gives the texture. With the templated grain growth from tape-casting, the temperature increases the achieved orientation [50]. The piezoelectric properties of the textured ceramics increase when they are measured in the ferroelectric a-b plane. Thus, Hong et al. have reported [51] an increase from 20 to 30 pC/N in Nb-doped $Bi_4Ti_3O_{12}$ ceramics in random and textured ceramics with Lotgering factors >0.96, as shown in Figure 7. Similar results have been published by other authors in different compositions with this structure. Thus, Jones et al. reported a d_{33} increase from 15 to 30 pC/N in $Na_{0.5}Bi_{4.5}Ti_4O_{12}$ [52]; Tamura et al. achieved an increase from 12.6 to 25 pC/N in Mn-doped $CaBi_4Ti_4O_{15}$ ceramics [53].

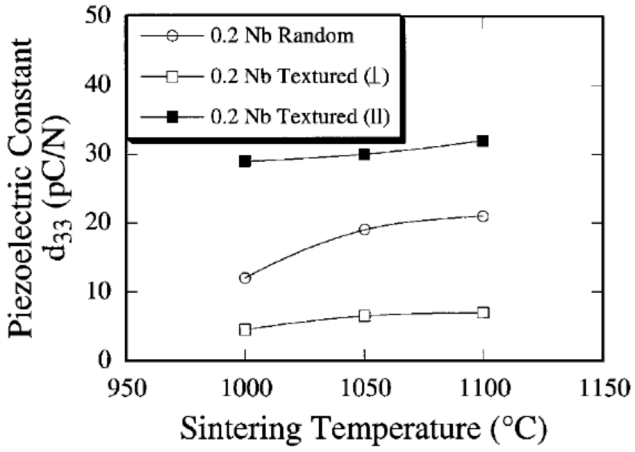

Figure 7. Piezoelectric constant, d_{33}, of the random and textured Nb-doped $Bi_4Ti_3O_{12}$ sintered for 2 h showing the anisotropy of the piezoelectric properties (taken from [51]).

Besides tape-casting techniques, there are other methods for texturing Aurivillius-type ceramics. For instance, Li et al. used the Rolling extended method to prepare $Ca_{0.85}(LiCe)_{0.075}Bi_4Ti_4O_{15}$ (LCCBT) textured ceramics with a templated grain growth [54]. In this technique, a clay-like paste containing the template and the matrix particles is forced to pass through a pair of rollers that produce the alignment of the anisometric particles. Lotgering factors of 0.93 were achieved. The d_{33} value measured in the a-b plane is 29.5 pC/N, while for random ceramics it is 18 pC/N. Shen et al. used a method called Superplastic-Deformation-Induced directional dynamic ripening to have grain-oriented $Bi_4Ti_3O_{12}$ ceramics [55]. They take advantage of the superplasticity properties of nanostructured materials before the T_g temperature of grain growth. By a subsequent SPS process, the authors were able to orientate the grains and promote their growth at 1000 °C. Lotgering factors of 0.985 were accomplished, with d_{33} values of 17.6 pC/N.

It is clear that the texture increases the piezoelectric properties if they are measured in the appropriate direction. However, the texture obtained by any of these methods is detrimental for the simultaneous appearance of good mechanical and ferroelectric properties. The resulting microstructure with the grain alignment favors the crack propagation along grain boundaries and through the a-b plane. The mechanical properties were shown to worsen for several Aurivillius phases [56]. Besides, the direction with the largest piezoelectric activity is the same as the maximal conductivity [57], which makes the unavoidable poling process and the application of potential devices at high temperature more difficult.

2.2. Doping Strategies

A route followed during several years to increase the piezoelectric coefficients in sintered ceramics is the doping of the structure. Values of d_{33} higher than 30 pC/N have been published for titanates and niobates Aurivillius with different number of pseudo-perovskites layers by this strategy. Thus, Wang et al. reported a value of d_{33} = 37 pC/N in a ceramic with multi-substitution $Li_{0.04}Ce_{0.04}Na_{(0.46-x/2)}Bi_{(4.46+x/2)}Ti_{(4-x)}Sc_xO_{15}$ after a thermal treatment in oxygen atmosphere [58]. Wang et al. achieved values of d_{33} = 33 pC/N for $Na_{0.5}Bi_{4.5}Ti_4O_{15}$ doped with Co [59]. d_{33} values of 31 pC/N have been also reported for $Na_{0.5}La_{0.5}Bi_2Nb_{2-x}W_xO_9$ [60] and $(Li,Nd,Ce)_{0.06}(Na,Bi)_{0.44}Bi_2Nb_2O_9$ [61] compositions. The reasons for the piezoelectric improvement by doping are the enhancement in local lattice distortion caused by LiNd and LiLa co-substitution and the high applied field due to fewer defects, as oxygen vacancies in the perovskite layers, which reduces the electrical conductivity. This leads to an increase of remnant polarization by reducing the leakage current. Cao et al. reported d_{33} values of 30 pC/N in $SrBi_4Ti_4O_{15}$ doped with Mn [62]. The enhanced piezoelectric performance can be attributed to the substitution of B-site Ti^{4+} ions by Mn^{3+} ions, which

induced BO_6 distortions. In addition, large grain size and high bulk densities reduced dielectric loss, contributing to the enhancement of the piezoelectric activity. All these coefficients were accomplished in materials with Curie temperature ranging from 500 to 796 °C. In those works, the authors prove that the ceramics are not depoled up to the transition temperature but the piezoelectric coefficients are not given at the potential working temperature. However, it is known that the piezoelectric activity decreases as the temperature increases, although values are high enough to allow their uses as high temperature piezoelectrics [63], as can be observed in Figure 8.

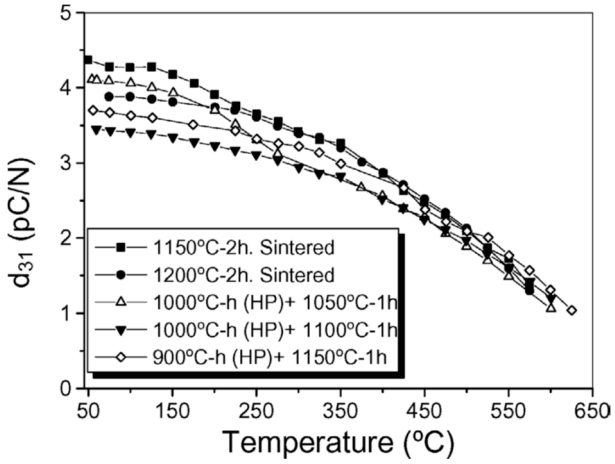

Figure 8. Thermal evolution of the real part of the piezoelectric coefficient d_{31} for recrystallized and sintered ceramics (taken from [63]).

3. Thin Films

The high coercive field can make difficult the needed poling for the Aurivillius structures, which can be a drawback for the potential applications for these materials. In this sense, the use of thin films can overcome this issue, besides expanding the applicability for this family of compounds. By reducing the material thickness, lower voltages (tens of V) are needed to apply a high electric field. This can help to facilitate the films integration in microelectronic devices.

The ferroelectric properties in Aurivillius thin films depend on several parameters as composition, microstructure or crystallographic orientation, which in turn is markedly dependent on the substrate. Different processing routes have been used during years to fabricate the thin films. Among them, sol-gel and spin-coating, Metal Organic Decomposition, Chemical Solution Deposition, Pulsed Laser Deposition or Magnetron Sputtering can be highlighted, at temperatures ranging from 600 to 800 °C. The peculiar dependence of the ferroelectric polarization with the crystalline structure and the anisotropic growth habit mark the dependence of the properties with the film texture. Thus, films with grains growing with the c-axis in normal to the substrates will have a very low spontaneous polarization in the normal plane [64], which will make the application more difficult. On the contrary, grains align with the a (or b) axis in the normal direction will maximize the ferroelectric response. This is the case of the work by Lee et al., which showed a remnant polarization of 32 $\mu C/cm^2$ in $Bi_{3.25}La_{0.75}Ti_3O_{12}$. The substrate determines the preferential growth by the adequate lattice matching with the film. Thus, a (100)-oriented growth of BLT was achieved using a YSZ(100) single-crystal substrates covered by a thin strained (110)-oriented $SrRuO_3$ layer. The strain increases $SrRuO_3$ lattice parameter, reducing the BLT-$SrRuO_3$ lattice misfit along the BLT[001]\$SrRuO_3$ [001] direction. It favors a better nucleation conditions for the growth of (100)-oriented BLT grains [65]. At least, a mixed orientation is needed to have a ferroelectric signal [64]. High values of remnant polarization were achieved in other doped $Bi_4Ti_3O_{12}$-based materials, i.e., 44 $\mu C/cm^2$ by Zr doping [66] or 19 $\mu C/cm^2$ in $Bi_{3.15}Nd_{0.85}Ti_3O_{12}$ thin films [67]. Other Aurivillius compositions have also been prepared and

characterized. Thus, Watanabe et al. processed thin films with $SrBi_2Nb_2O_9$, $SrBi_2Ta_2O_9$, $SrBi_4Ti_4O_{15}$ and different solid solutions among them. Maxima values of 19 and 25 μC/cm^2 were achieved in $(SrBi_2Nb_2O_9)_{0.80}$-$(SrBi_2Ta_2O_9)_{0.20}$ and $(SrBi_2Ta_2O_9)_{0.80}$-$(SrBi_4Ti_4O_{15})_{0.20}$, respectively [68]. Lettieri et al. reported values of P_r = 15.7 μC/cm^2 in non c-oriented $SrBi_2Nb_2O_9$ films [69] (Figure 9).

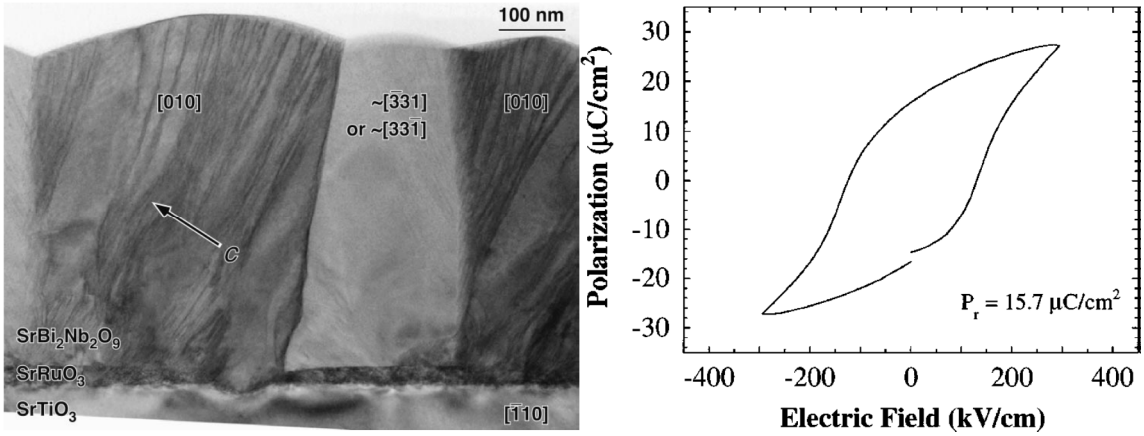

Figure 9. Cross-sectional TEM image along the [110] $SrTiO_3$ zone axis of the same (103)$SrBi_2Nb_2O_9$/(111) $SrRuO_3$/(111) $SrTiO_3$ film from which the Polarization–electric-field hysteresis curve shown at the right Figure was measured (taken from [69]).

The interest in Aurivillius thin films is also related to the fatigue-free characteristics for this family of compounds. Fatigue is the ability of the material to cyclically switch its ferroelectric polarization without reducing the amount of switched charge. This property makes this material a potential candidate for nonvolatile ferroelectric random access memory FeRAM applications. The positive and negative polarization can be taken as "1" and "0" states. There are several advantages with respect to traditional memories, as high speeds or low voltages needed for the data writing. The non-volatility allows avoiding the energy needed for the data retention. For its use, it is essential to have high remnant polarization and the ability to make the writing-erasing operation for long times without properties degradation, thus is, being a fatigue-free material. After the work by Araujo et al. [70], who reported 10^{12} cycles without appreciable loss of polarization, several works were focused on the enhancement of this characteristic. Values ranging from 10^{10} to 10^{12} cycles have been reported for different Aurivillius compositions, as $(Bi_{3.54}Nd_{0.46})Ti_3O_{12}$ [71], $Sr_{0.8}Bi_{2.2}Ta_2O_9$ [72] or $Bi_{3.75}La_{0.25}Ti_3O_{12}$ [73]. The oxygen vacancies play an important role for this property. They are more commonly located at the Bi_2-O_2 layers, rather than in the perovskite blocks. Their influence in the polarization loss is then lower. In addition, and mainly with Pt electrodes, the number of oxygen vacancies at the ferroelectric/electrode interfaces is lower than in perovskite ferroelectrics, which leads to a better polarization fatigue behavior. However, there are some drawbacks with these materials for this application, as the high leakage currents or the difficult integration with Si-based system. By now, FeRAM is only a potential and not real application.

4. Applications

4.1. High Temperature Piezoelectricity

As ferroelectric materials, Aurivillius compounds are piezoelectric after electrical poling. Two characteristics are exploited: their high ferro-paraelectric phase transitions, which make them good candidates for uses as high temperature piezoelectrics; and the high coercive fields, which facilitate the uses as actuators with difficult depolarization.

Nowadays, the Ferroperm company is commercializing bismuth titanate ceramics (code Pz46, with values of d_{33} = 18 pC/N; d_{31} = 2 pC/N; K_t = 0.20; T_C = 650 °C) [74]. It is recommended mainly for high temperature applications, as flow-meters or pressure sensors.

There are two main applications for piezoelectrics at high temperature: as sensors or as transducers [75]. Thus, as sensors, *accelerometers* are used to detect abnormal behaviors in combustion engines working at harsh conditions, at high pressure (80 bars) and high temperature (1.227 °C); *high temperature SAW* (Surface Acoustic Wave) sensors can be suitable for monitoring temperatures, pressures or gas concentrations for high-temperature applications such as HT furnaces or process chambers for semiconductors or ceramics manufacturing. The possibility of using wireless systems without traditional thermocouples or thermistors makes HT SAW a promising technique for these high-temperature applications, as shown in Figure 9 in reference [75]; *Acoustic Emission Sensor*. The generation of a crack or its propagation produces the release of elastic energy that can be detected by means of piezoelectric sensors. High-temperature non-destructive inspection techniques are frequently required for particular applications such as the nuclear power industry, for safety reasons; *Gas Sensor*. By monitoring the shifts in resonance frequency produced by changes in mass, the gas molecules absorbed at the surface can be detected, for example in high-temperature combustion processes; *Pressure Sensor*. They are commonly used in internal combustion engines and turbines, with high pressures and temperatures.

In the case of actuators or transducers, applications can be found as ultrasound transducers for non-destructive testing (NDT) and non-destructive evaluation (NDE) in high-temperature environments. In this sense, potential applications have generated an important interest in the field of Space exploration. The working conditions in the Solar System can be very extreme. Temperatures in Venus can be as high as 460 °C. Most of the currently available electronic electromagnetic actuators are limited in their ability to produce sufficiently high stroke, torque, o3r force at the extreme conditions, which can be achieved by electromechanical devices. The actuators that are needed for robotic exploration include lander pedal motors, drive/steering motors, manipulator joint motors, latching and deployment motors and sampling tool motors [76]. Some of these applications are motors as important elements of automatic and robotic mechanisms.

As examples in this field of Space exploration, Bao et al. from the Jet Propulsion Laboratory at NASA published the study of a high temperature piezoelectric drill, as the one shown in [77]. In that work, the authors designed a testbed to simulate the conditions in Venus. Basalt or brick samples were drilled at 500 °C by a piezoelectric drill with different piezoelectric materials for the transducer that drives the USDC. They found advantages in the use of bismuth titanate in terms of drilling depth and time duration over other materials as $LiNbO_3$. This opened new perspectives for high temperatures applications for Aurivillius in Space exploration.

4.2. Multiferroism

The magnetoelectric (ME) multiferroics (MF) materials are defined as those possessing simultaneously ferroelectric and ferromagnetic properties and exhibit linear coupling. They can present them in a single phase or in composites and layered thin films. The interest for this property is mainly due to that magnetic properties could be controlled by electric fields, which would simplify the devices and the energy needed, for example, in process of write/read information.

There are scarce single phase materials that can present simultaneously ferroelectric and ferromagnetic properties above room temperature [78]. An example is $BiFeO_3$, an antiferromagnetic and ferroelectric material with a Curie temperature close to 1100 K and Neel temperature T_N near 625 K [79].

Aurivillius-type structures have been proposed as good candidates for use as single phase multiferroic materials because of their high ferro-paraelectric phase transition temperatures and the ease hosting of "magnetic cations" in the structure. The research has been focused on compositions with cobalt and iron, for which weak or strong ferromagnetic behavior above room temperature have been found. Many articles

show that phases containing Fe and Co have simultaneously ferroelectric and ferromagnetic properties above room temperature. Relative high values of Pr between 13 and 16 μC/cm^2 have been achieved in $Bi_6Fe_{2-x}Co_xTi_3O_{18}$ solid solutions and $Bi_5Ti_3FeO_{15}$ compositions [80–82]. A common characteristic is that the ferroelectric saturation is hard to achieve. However, the works that show magneto-electric effect (that is, a real interaction between two orders, which is the property to be explored) are scarcer to be found [83–85]. In those works, very weak coupling is shown but they prove that at least a way is open in this direction. In fact, multiferroic applications are now far from the practical point of view (not only for Aurivillius compounds).

4.3. Photocatalytic

Beside the applications based on the piezoelectric properties of bismuth layered ferroelectric materials, efforts have been carried out to explore other characteristics of this family of materials as the photocatalytic activity. TiO_2 has been widely used as a photocatalyst for energy conversion and pollutant elimination because of its high activity and stability, low cost, availability and nontoxicity [86]. However, it is only activated under UV radiation, because of its large band gap (about 3.2 eV). Thus, alternatives are considered. $Bi_4Ti_3O_{12}$ has been proposed, with a relatively high photocatalyst activity attributed to the effective utilization of interlayer space as reaction sites [87]. Examples that show the potential of $Bi_4Ti_3O_{12}$ for this type of applications can be found in the photodegradation of methyl orange [84,88]. The photocatalytic activity is high, although lower than for TiO_2. In can be improved by selective doping, as in the case of Cr [86]. Further improvement could be achieved by reducing the electron-hole combination (promoting the appearance of oxygen vacancies, for instance) or increasing the light absorption. It has been also shown that the use of $Bi_4Ti_3O_{12}$ nanofibers can also give a better photocatalytic activity [89].

5. Perspectives of Aurivillius Materials as Lead Free Piezoelectrics

Aurivillius type structure materials have a number of characteristics that condition their applications in different fields. In terms of piezoelectric activity at room temperature, they are quite far from other lead free piezoelectric compositions. While the highest d_{33} coefficients reach values no higher than 40 pC/N (even in textured ceramics), other families of compositions reach very much higher values [90]. Thus, within the solid solution $BaTiO_3$-$BaZrO_3$-$CaTiO_3$ (BCZT), the composition $Ba(Zr_{0.15}Ti_{0.85})O_3$-$x(Ba_{0.8}Ca_{0.2})TiO_3$ has shown values up to d_{33} = 620 pC/N [91]. For the $(Bi_{0.5}Na_{0.5})TiO_3$-$BaTiO_3$ (BNT-BT) system, values of d_{33} = 180 pC/N have been achieved for the $(Bi_{0.5}Na_{0.5})_{0.94}Ba_{0.06}TiO_3$ compositions. With respect to the families of niobates with $(K_{0.5}Na_{0.5})NbO_3$ (KNN) based composition, a high value of d_{33} = 490 pC/N was recently reported for a $0.96(K_{0.48}Na_{0.52})(Nb_{0.97}Sb_{0.03})O_3$–$0.04Bi_{0.5}(Na_{0.82}K_{0.18)0.5}ZrO_3$) solid solution [92].

It seems obvious that the piezoelectric activity for Aurivillius compounds at room temperature is not competitive with other piezoelectric lead-free materials in terms of applications where high piezoelectric coefficients are essential. The d_{33} values are one order of magnitude lower in some cases. However, the high coercive fields for Aurivillius ferroelectrics could make them good candidates for actuators applications, because the depoling by the application of an electrical field is difficult, even at room temperature.

There are other properties for Aurivillius compounds that allow to have their own potential niches as lead-free piezoelectric applications. The most characteristic property for Aurivillius compounds is their high ferro-paraelectric transition temperature, which in some cases can be higher than 900 °C (as for Bi_3TiNbO_9). It is in these applications (at temperatures higher than 500 °C) where this family of materials can be competitive as lead-free piezoelectrics. They cover several fields as aerospace and aircraft industries, nuclear power plants, wind power and geothermal power. In all of these cases, sensors working at high temperature can be useful for in situ inspection and monitoring [93]. In these cases, other materials must be compared with Aurivillius compounds, as quartz, Langasite and Oxyborate. In all these cases, these materials can be used only as single crystals, due to the difficulties

of obtaining ceramics with their compositions. Besides the difficulties of working with single crystals, their piezoelectric activity is lower than for Aurivillius compounds. Besides, Aurivillius compounds can have potential applications in no piezoelectric fields, as photocatalytic or multiferroic materials, as explained before.

Acknowledgments: Alberto Moure is indebted to MINECO for the "Ramon y Cajal" contract (Ref. RYC-2013-14436), which is co-financed with European Social Fund.

Conflicts of Interest: The authors declare no conflict of interest.

References

1. Aurivillius, B. Mixed bismuth oxides with layer lattices. *Arkiv Kemi* **1949**, *1*, 463–480.
2. Fukunaga, M.; Takesada, M.; Onodera, A. Ferroelectricity in layered perovskites as a model of ultra-thin films. *World J. Condens. Matter Phys.* **2016**, *6*, 224–243. [CrossRef]
3. Rae, A.D.; Thompson, J.G.; Withers, R.L. Structure refinement of commensurately modulated bismuth tungstate, Bi_2WO_6. *Acta Cryst.* **1991**, *B47*, 870. [CrossRef]
4. Thompson, J.G.; Rae, A.D.; Withers, R.L.; Craig, D.C. Revised structure of Bi_3TiNbO_9. *Acta Cryst.* **1991**, *B46*, 174–180. [CrossRef]
5. Rae, A.D.; Thompson, J.G.; Withers, R.L. Structure refinement of commensurately modulated bismuth titanate, $Bi_4Ti_3O_{12}$. *J. Solid State Chem.* **1991**, *94*, 474–487. [CrossRef]
6. Pardo, L.; Castro, A.; Millán, P.; Alemany, C.; Jiménez, R.; Jiménez, B. $(Bi_3TiNbO_9)_x(SrBi_2Nb_2O_9)_{1-x}$ Aurivillius type structure piezoelectric ceramics obtained from mechanochemically activated oxides. *Acta Mater.* **2000**, *48*, 2421–2428. [CrossRef]
7. Xu, G.; Yang, Y.; Bai, H.; Wang, J.; Tian, H.; Zhao, R.; Wei, X.; Yanga, X.; Han, G. Hydrothermal synthesis and formation mechanism of the single-crystalline $Bi_4Ti_3O_{12}$ nanosheets with dominant (010) facets. *Cryst. Eng. Commun.* **2016**, *18*, 2268–2274. [CrossRef]
8. Wang, F.; Wang, J.; Zhong, X.; Li, B.; Liu, J.; Wu, D.; Mo, D.; Guo, D.; Yuan, S.; Zhang, K.; et al. Shape-controlled hydrothermal synthesis of ferroelectric $Bi_4Ti_3O_{12}$ nanostructures. *Cryst. Eng. Commun.* **2013**, *15*, 1397–1403. [CrossRef]
9. Yang, Q.; Li, Y.; Yin, Q.; Wang, P.; Cheng, Y.B. $Bi_4Ti_3O_{12}$ nanoparticles prepared by hydrothermal synthesis. *J. Eur. Ceram. Soc.* **2003**, *23*, 161–166. [CrossRef]
10. Shi, Y.; Cao, C.; Feng, S. Hydrothermal synthesis and characterization of $Bi_4Ti_3O_{12}$. *Mater. Lett.* **2000**, *46*, 270–273. [CrossRef]
11. Li, X.; Ju, Z.; Li, F.; Huang, Y.; Xie, Y.; Fu, Z.; Knized, R.J.; Lu, Y. Visible light responsive $Bi_7Fe_3Ti_3O_{21}$ nanoshelf photocatalysts with ferroelectricity and ferromagnetism. *J. Mater. Chem. A* **2014**, *2*, 13366–13372. [CrossRef]
12. Xie, D.; Pan, W. Study on $BaBi_4Ti_4O_{15}$ nanoscaled powders prepared by sol–gel method. *Mater. Lett.* **2003**, *57*, 2970–2974. [CrossRef]
13. Wisedsri, R.; Chaisuwan, T.; Wongkasemjit, S. Simple route to bismuth titanate from bismuth glycolate precursor via sol–gel process. *Mater. Res. Innov.* **2013**, *17*, 43–48. [CrossRef]
14. Koch, R.J.; Lokuhewa, I.N.; Shi, J.; Haluska, M.S.; Misture, S.T. Chemical synthesis of nanoscale Aurivillius ceramics, $Bi_2A_2TiM_2O_{12}$ (A=Ca, Sr, Ba and M=Nb, Ta). *J. Sol. Gel. Sci. Technol.* **2012**, *64*, 612–618. [CrossRef]
15. Babooram, K.; Chin, D.K.; Ye, Z.-G. Ferroelectric $Bi_4Ti_3O_{12}$ and $Bi_{4-x}La_xTi_3O_{12}$ ceramics prepared by a new sol-gel route. *J. Electroceram.* **2008**, *21*, 43–48. [CrossRef]
16. Hardy, A.; Mondelaers, D.; Van Bael, M.K.; Mullens, J.; Van Poucke, L.C.; Vanhoyland, G.; D'Haen, J. Synthesis of $(Bi, La)_4Ti_3O_{12}$ by a new aqueous solution-gel route. *J. Eur. Ceram. Soc.* **2004**, *24*, 905–909. [CrossRef]
17. Shi, M.; Shi, Y.; Zuo, R.; Xu, Y.; Peng, X.; Li, D.; Xie, L. Microstructure, ferroelectric and dielectric proprieties of $Bi_4Ti_3O_{12}$ materials prepared by two methods. *J. Mater. Sci. Mater. Electron.* **2016**, *27*, 3361–3367. [CrossRef]
18. Villegas, M.; Moure, C.; Fernandez, J.F.; Duran, P. Low-temperature sintering of submicronic randomly oriented $Bi_4Ti_3O_{12}$ materials. *Ceram. Int.* **1996**, *22*, 15–22. [CrossRef]

19. Lisoni, J.G.; Millán, P.; Vila, E.; Martín de Vidales, J.L.; Hoffmann, T.; Castro, A. Synthesis of ferroelectric $Bi_4Ti_3O_{12}$ by alternative routes: Wet no-coprecipitation chemistry and mechanochemical activation. *Chem. Mater.* **2001**, *13*, 2084–2091. [CrossRef]
20. Du, Y.; Fang, J.; Zhang, M.; Hong, J.; Yin, Z.; Zhang, Q. Phase character and structural anomaly of $Bi_4Ti_3O_{12}$ nanoparticles prepared by chemical coprecipitation. *Mater. Lett.* **2002**, *57*, 802–806. [CrossRef]
21. Chen, Z.-H.; Qiu, J.-F.; Liu, C.; Ding, J.-N.; Zhu, Y.-Y. Preparation of $Bi_4Ti_3O_{12}$ nanopower by azeotropic co-precipitation and dielectric properties of the sintered ceramic. *Ceram. Int.* **2010**, *36*, 241–244.
22. Kong, L.B.; Ma, J.; Zhu, W.; Tan, O.K. Preparation of $Bi_4Ti_3O_{12}$ ceramics via a high-energy ball milling process. *Mater. Lett.* **2001**, *51*, 108. [CrossRef]
23. Sim, M.H.; Xue, J.M.; Wang, J. Layer structured calcium bismuth titanate by mechanical activation. *Mater. Lett.* **2004**, *58*, 2032–2036. [CrossRef]
24. Ng, S.H.; Xue, J.M.; Wang, J. High temperature piezoelectric strontium bismuth titanate from mechanical activation of mixed oxides. *Mater. Chem. Phys.* **2002**, *75*, 131–135. [CrossRef]
25. Moure, A.; Pardo, L.; Alemany, C.; Millán, P.; Castro, A. Piezoelectric ceramics based on Bi_3TiNbO_9 from mechanochemically activated precursors. *J. Eur. Ceram. Soc.* **2001**, *21*, 1399–1402. [CrossRef]
26. Ferrer, P.; Iglesias, J.E.; Castro, A. Synthesis of the Aurivillius phase $SrBi_4Ti_4O_{15}$ by a mechanochemical activation route. *Chem. Mater.* **2004**, *16*, 1323–1329. [CrossRef]
27. Berbenni, V.; Milanese, C.; Bruni, G.; Girella, A.; Marini, A. Synthesis of $Bi_4Ti_3O_{12}$ by high energy milling of Bi_2O_3–TiO_2 (anatase) mixtures. *J. Therm. Anal. Calorim.* **2016**, *126*, 1507. [CrossRef]
28. Moure, A.; Castro, A.; Pardo, L. Improvement by recrystallisation of Aurivillius-type structure piezoceramics from mechanically activated precursors. *Acta Mater.* **2004**, *52*, 945–957. [CrossRef]
29. Kan, Y.; Jin, X.; Wang, P.; Li, Y.; Cheng, Y.B.; Yan, D. Anisotropic grain growth of $Bi_4Ti_3O_{12}$ in molten salt fluxes. *Mater. Res. Bull.* **2003**, *38*, 567–576. [CrossRef]
30. Xiang, P.H.; Kinemuchi, Y.; Watari, K. Synthesis of layer-structured ferroelectric Bi_3NbTiO_9 plate-like seed crystals. *Mater. Let.* **2005**, *59*, 1876–1879. [CrossRef]
31. Porob, D.G.; Maggard, P.A. Synthesis of textured $Bi_5Ti_3FeO_{15}$ and $LaBi_4Ti_3FeO_{15}$ ferroelectric layered Aurivillius phases by molten-salt flux methods. *Mater. Res. Bull.* **2006**, *41*, 1513–1519. [CrossRef]
32. Tang, Q.Y.; Kan, Y.M.; Wang, P.L.; Li, Y.G.; Zhang, G.J. Nd/V Co-Doped $Bi_4Ti_3O_{12}$ powder prepared by molten salt synthesis. *J. Am. Ceram. Soc.* **2007**, *90*, 3353–3356. [CrossRef]
33. Chang, Y.; Wu, J.; Yang, B.; Zhang, S.; Lv, T.; Cao, W. Synthesis and properties of high aspect ratio $SrBi_4Ti_4O_{15}$ microplatelets. *Mater. Lett.* **2014**, *129*, 126–129. [CrossRef]
34. He, H.; Yin, J.; Li, Y.; Zhang, Y.; Qiu, H.; Xu, J.; Xu, T.; Wang, C. Size controllable synthesis of single-crystal ferroelectric $Bi_4Ti_3O_{12}$ nanosheet dominated with {0 0 1} facets toward enhanced visible-light-driven photocatalytic activities. *Appl. Catal. B* **2014**, *156–157*, 35–43. [CrossRef]
35. Kumar, S.; Panneerselvam, M.; Vinatier, P.; Rao, K.J. Microwave synthesis and sintering of $Bi_4Ti_3O_{12}$, the Aurivillius compound: Structural and chemical effects of attempted lithiation. *Ferroelectrics* **2004**, *306*, 165–177. [CrossRef]
36. Rocha, G.N.; Melo, L.F.L.; Castro, M.C., Jr.; Ayala, A.P.; de Menezes, A.S.; Fechine, P.B.A. Structural characterization of bismuth rare earth tungstates obtained by fast microwave-assisted solid-state synthesis. *Mater. Chem. Phys.* **2013**, *139*, 494–499. [CrossRef]
37. Hao, H.; Liu, H.; Liu, Y.; Cao, M.; Ouyang, S. Lead-Free $SrBi_4Ti_4O_{15}$ and $Bi_4Ti_3O_{12}$ material fabrication using the microwave-assisted molten salt synthesis method. *J. Am. Ceram. Soc.* **2007**, *90*, 1659–1662. [CrossRef]
38. Thomazini, D.; Gelfuso, M.V.; Eiras, J.A. Microwave assisted hydrothermal synthesis of $Bi_4Ti_3O_{12}$ nanopowders from oxide as raw materials. *Powder Technol.* **2012**, *222*, 139–142. [CrossRef]
39. Takenaka, T.; Sakata, K. Grain orientation and electrical properties of hot-forged $Bi_4Ti_3O_{12}$ ceramics. *Jpn. J. Appl. Phys.* **1980**, *19*, 31. [CrossRef]
40. Igarashi, H.; Matsunaga, J.; Taniai, T.; Okazaki, K. Dielectric and piezoelectric properties of grain-oriented $PbBi_2Nb_2O_9$ ceramics. *Am. Ceram. Soc. Bull.* **1978**, *57*, 815.
41. Adamczyk, M.; Kozielski, L.; Pawełczyk, M. Effect of hot pressing on processing and properties of BBN ceramics. *Ceram. Int.* **2008**, *34*, 1617. [CrossRef]
42. Chen, H.; Shen, B.; Xu, J.; Kong, L.; Zhai, J. Correlation between grain sizes and electrical properties of $CaBi_2Nb_2O_9$ piezoelectric ceramics. *J. Am. Ceram. Soc.* **2012**, *95*, 3514–3518. [CrossRef]

43. Hungría, T.; Galy, J.; Castro, A. Spark Plasma Sintering as a useful technique to the nanostructuration of piezo-ferroelectric materials. *Adv. Eng. Mater.* **2009**, *11*, 615–631. [CrossRef]
44. Yan, H.; Zhang, H.; Ubic, R.; Reece, M.J.; Shen, Z.; Zhang, Z. A lead-free high-Curie-point ferroelectric ceramic, $CaBi_2Nb_2O_9$. *Adv. Mater.* **2005**, *17*, 1261–1265. [CrossRef]
45. Liu, J.; Shen, Z.; Nygren, M.; Kanb, Y.; Wang, P. SPS processing of bismuth-layer structured ferroelectric ceramics yielding highly textured microstructures. *J. Eur. Ceram. Soc.* **2006**, *26*, 3233–3239. [CrossRef]
46. Zhang, Z.; Yan, H.; Xiang, P.; Dong, X.; Wang, Y. Grain orientation effects on the properties of a bismuth layer-structured ferroelectric (BLSF) Bi_3NbTiO_9 Solid Solution. *J. Am. Ceram. Soc.* **2004**, *87*, 602–605. [CrossRef]
47. Liu, L. Progress on the fabrication of lead-free textured piezoelectric ceramics: Perspectives over 25 years. *J. Mater. Sci. Mater. Electron.* **2015**, *26*, 4425–4437. [CrossRef]
48. Messing, G.L.; Trolier-McKinstry, S.; Sabolsky, E.M.; Duran, C.; Kwon, S.; Brahmaroutu, B.; Park, P.; Yilmaz, H.; Rehrig, P.W.; Eitel, K.B.; et al. Templated grain growth of textured piezoelectric ceramics. *Crit. Rev. Solid State Mater. Sci.* **2004**, *29*, 45–96. [CrossRef]
49. Horn, J.A.; Zhang, S.C.; Selvaraj, U.; Messing, G.L.; Trolier-McKinstry, S. Templated grain growth of textured bismuth titanate. *J. Am. Ceram. Soc.* **1999**, *82*, 921–926. [CrossRef]
50. Kan, Y.; Wang, P.; Li, Y.; Cheng, Y.B.; Yan, D. Fabrication of textured bismuth titanate by templated grain growth using aqueous tape casting. *J. Eur. Ceram. Soc.* **2003**, *23*, 2163–2169. [CrossRef]
51. Hong, S.H.; Trolier-McKinstry, S.; Messing, G.L. Dielectric and electromechanical properties of textured niobium-doped bismuth titanate ceramics. *J. Am. Ceram. Soc.* **2000**, *83*, 113–118. [CrossRef]
52. Jones, J.L.; Iverson, B.J.; Bowman, K.J. Texture and Anisotropy of Polycrystalline Piezoelectrics. *J. Am. Ceram. Soc.* **2007**, *90*, 2297–2314. [CrossRef]
53. Tamura, K.; Kimura, T. Tailoring of grain size in textured $CaBi_4Ti_4O_{15}$ ceramics prepared by templated grain growth process. *J. Am. Ceram. Soc.* **2012**, *95*, 3421–3427. [CrossRef]
54. Li, T.; Li, X.; Zhao, Z.; Dai, Y.; Ji, H. Evolution of textured $Ca_{0.85}(LiCe)_{0.075}Bi_4Ti_4O_{15}$ ceramics via templated grain growth using a rolling-extended method. *J. Mater. Sci. Mater. Electron.* **2015**, *26*, 2082–2089. [CrossRef]
55. Shen, Z.; Liu, J.; Grins, J.; Nygren, M.; Wang, P.; Kan, Y.; Yan, H.; Sutter, U. Effective grain alignment in $Bi_4Ti_3O_{12}$ ceramics by superplastic-deformation-induced directional dynamic ripening. *Adv. Mater.* **2005**, *17*, 676–680. [CrossRef]
56. Moure, A.; Castro, A.; Pardo, L. Aurivillius-type ceramics, a class of high temperature piezoelectric materials: Drawbacks, advantages and trends. *Prog. Solid State Chem.* **2009**, *37*, 15–39. [CrossRef]
57. Cummins, S.E.; Cross, L.E. Electrical and pptical properties of ferroelectric $Bi_4Ti_3O_{12}$ single crystals. *J. Appl. Phys.* **1968**, *39*, 2268–2274. [CrossRef]
58. Wang, Q.; Fan, H.; Long, C.; Huang, L. Crystal structure and thermal annealing behaviors of high d_{33} Aurivillius-phase ceramics $Li_{0.04}Ce_{0.04}Na_{(0.46-x/2)}Bi_{(4.46+x/2)}Ti_{(4-x)}Sc_xO_{15}$ with the Sc^{3+}/Bi^{3+} co-substitution. *J. Mater. Sci. Mater. Electron.* **2014**, *25*, 2961–2968. [CrossRef]
59. Wang, C.M.; Zhao, L.; Liu, Y.; Withers, R.L.; Zhang, S.; Wang, Q. The temperature-dependent piezoelectric and electromechanical properties of cobalt-modified sodium bismuth titanate. *Ceram. Int.* **2016**, *42*, 4268–4273. [CrossRef]
60. Long, C.; Fan, H.; Li, M.; Li, Q. Effect of lanthanum and tungsten co-substitution on the structure and properties of new Aurivillius oxides $Na_{0.5}La_{0.5}Bi_2Nb_{2-x}W_xO_9$. *Cryst. Eng. Commun.* **2012**, *14*, 7201–7208. [CrossRef]
61. Long, C.; Fan, H.; Li, M. High temperature Aurivillius piezoelectrics: The effect of (Li, Ln) modification on the structure and properties of $(Li, Ln)_{0.06}(Na, Bi)_{0.44}Bi_2Nb_2O_9$ (Ln = Ce, Nd, La and Y). *Dalton Trans.* **2013**, *42*, 3561–3570. [CrossRef] [PubMed]
62. Cao, Z.P.; Wang, C.M.; Lau, K.; Wang, Q.; Fu, Q.W.; Tian, H.H.; Yin, D.F. Large enhancement of piezoelectric properties in Mn-modified $SrBi_4Ti_4O_{15}$ and its thermal stabilities at elevated temperatures. *Ceram. Int.* **2016**, *42*, 11619–11625. [CrossRef]
63. Moure, A.; Alemany, C.; Pardo, L. Temperature dependence of piezoelectric, elastic and dielectric coefficients at radial resonance of piezoceramics with an Aurivillius-type structure. *IEEE Trans. Ultrason. Ferroelectr. Freq. Control* **2005**, *52*, 570–577. [CrossRef] [PubMed]

64. Pignolet, A.; Schäfer, C.; Satyalakshmi, K.M.; Harnagea, C.; Hesse, D.; Gösele, U. Orientation dependence of ferroelectricity in pulsed-laser-deposited epitaxial bismuth-layered perovskite thin films. *Appl. Phys. A* **2000**, *70*, 283–291. [CrossRef]
65. Lee, H.N.; Hesse, D.; Zakharov, N.; Gösele, U. Ferroelectric $Bi_{3.25}La_{0.75}Ti_3O_{12}$ films of uniform a-axis orientation on silicon substrates. *Science* **2002**, *296*, 2006–2009. [CrossRef] [PubMed]
66. Chen, J.; Yun, Q.; Gao, W.; Bai, Y.; Nie, C.; Zhao, S. Improved ferroelectric and fatigue properties in Zr doped $Bi_4Ti_3O_{12}$ thin films. *Mater. Lett.* **2014**, *136*, 11–14. [CrossRef]
67. Guo, D.; Wang, C.; Shen, Q.; Zhang, L.; Li, M.; Liu, J. Effect of measuring factors on ferroelectric properties of $Bi_{3.15}Nd_{0.85}Ti_3O_{12}$ thin films prepared by sol–gel method for non-volatile memory. *Appl. Phys. A* **2009**, *97*, 877–881. [CrossRef]
68. Watanabe, H.; Mihara, T.; Yoshimori, H.; Paz de Araujo, C.A. Preparation of ferroelectric thin films of bismuth layer structured compounds. *Jpn. J. Appl. Phys.* **1995**, *34*, 5240. [CrossRef]
69. Lettieri, J.; Zurbuchen, M.A.; Jia, Y.; Schlom, D.G.; Streiffer, S.K.; Hawley, M.E. Epitaxial growth of non-c-oriented $SrBi_2Nb_2O_9$ on (111) $SrTiO_3$. *Appl. Phys. Lett.* **2000**, *76*, 2937. [CrossRef]
70. Paz de Araujo, C.A.; Cuchiaro, J.D.; McMillan, L.D.; Scott, M.C.; Scott, J.F. Fatigue-free ferroelectric capacitors with platinum electrodes. *Nature* **1995**, *374*, 627–629. [CrossRef]
71. Kojima, T.; Sakai, T.; Watanabe, T.; Funakubo, H.; Saito, K.; Osada, M. Large remanent polarization of $(Bi,Nd)_4Ti_3O_{12}$ epitaxial thin films grown by metalorganic chemical vapor deposition. *Appl. Phys. Lett.* **2002**, *80*, 2746–2748. [CrossRef]
72. Calzada, M.L.; Gonzalez, A.; Garcia-Lopez, J.; Jimenez, R. Crystallization, heterostructure, microstructure and properties of ferroelectric strontium bismuth tantalate films derived from tantalum glycolate solutions. *Chem. Mater.* **2003**, *15*, 4775–4783. [CrossRef]
73. Simões, A.Z.; Riccardi, C.S.; Cavalcante, L.S.; Longo, E.; Varela, J.A.; Mizaikoff, B.; Hess, D.W. Ferroelectric fatigue endurance of $Bi_{4-x}La_xTi_3O_{12}$ thin films explained in terms of *x*-ray photoelectron spectroscopy. *J. Appl. Phys.* **2007**, *101*, 084112. [CrossRef]
74. MEGGITT. Available online: http://www.ferroperm-piezo.com/files/files/Ferroperm%20Catalogue.pdf (accessed on 1 October2017).
75. Jiang, X.; Kim, K.; Zhang, S.; Johnson, J.; Salazar, G. High-Temperature Piezoelectric Sensing. *Sensors* **2014**, *14*, 144–169. [CrossRef] [PubMed]
76. Sherrit, S. Smart material/actuator needs in extreme environments in space. In Proceedings of the SPIE—The International Society for Optical Engineering, San Diego, CA, USA, 7–10 March 2005; Volume 5761, p. 335.
77. Bao, X.; Bar-Cohen, Y.; Sherrit, S.; Badescu, M.; Shrout, T. High temperature piezoelectric drill. In Proceedings of the SPIE—The International Society for Optical Engineering, San Diego, CA, USA, 3–4 August 2009; Volume 72922B.
78. Hill, N. Materials Why are there so few magnetic ferroelectrics? *J. Phys. Chem. B* **2000**, *104*, 6694–6709. [CrossRef]
79. Catalan, C.; Scott, J.F. Physics and applications of bismuth ferrite. *Adv. Mater.* **2009**, *21*, 2463. [CrossRef]
80. Mao, X.; Wang, W.; Chen, X.; Lu, Y. Multiferroic properties of layer-structured $Bi_5Fe_{0.5}Co_{0.5}Ti_3O_{15}$ ceramics. *Appl. Phys. Lett.* **2009**, *95*, 082901. [CrossRef]
81. Bai, W.; Gao, Y.Q.; Zhu, J.Y.; Meng, X.J.; Lin, T.; Yang, J.; Zhu, Z.Q.; Chu, J.H. Electrical, magnetic and optical properties in multiferroic $Bi_5Ti_3FeO_{15}$ thin films prepared by a chemical solution deposition route. *J. Appl. Phys.* **2011**, *109*, 064901. [CrossRef]
82. Maoa, X.; Suna, H.; Wanga, W.; Lub, Y.; Chen, X. Effects of Co-substitutes on multiferroic properties of $Bi_5FeTi_3O_{15}$ ceramics. *Solid State Commun.* **2012**, *152*, 483–487. [CrossRef]
83. Fuentes, L.; García, M.; Matutes-Aquino, J.; Ríos-Jara, D. Magnetoelectricity via crystallography. *J. Alloys Compd.* **2004**, *369*, 10–13. [CrossRef]
84. Keeney, L.; Maity, T.; Schmidt, M.; Amann, A.; Deepak, N.; Petkov, N.; Roy, S.; Pemble, M.E.; Whatmore, R.W. Magnetic field-induced ferroelectric switching in multiferroic Aurivillius phase thin films at room temperature. *J. Am. Ceram. Soc.* **2013**, *96*, 2339–2357. [CrossRef]
85. Zhao, Y.; Fan, H.; Liu, G.; Liu, Z.; Ren, X. Ferroelectric, piezoelectric properties and magnetoelectric coupling behavior in Aurivillius $Bi_5Ti_3FeO_{15}$ multiferroic nanofibers by electrospinning. *J. Alloys Compd.* **2016**, *675*, 441–447. [CrossRef]

86. Chen, Z.; Jiang, X.; Zhu, C.; Shi, C. Chromium-modified $Bi_4Ti_3O_{12}$ photocatalyst: Application for hydrogen evolution and pollutant degradation. *Appl. Catal. B* **2016**, *199*, 241–251. [CrossRef]
87. Yao, W.F.; Wang, H.; Xu, X.H.; Shang, S.X.; Hou, Y.; Zhang, Y.; Wang, M. Synthesis and photocatalytic property of bismuth titanate $Bi_4Ti_3O_{12}$. *Mater. Lett.* **2003**, *57*, 1899–1902. [CrossRef]
88. Yao, W.F.; Xu, X.H.; Wang, H.; Zhou, J.T.; Yang, X.N.; Zhang, Y.; Shang, S.X.; Huang, B.B. Photocatalytic property of perovskite bismuth titanate. *Appl. Catal. B* **2004**, *52*, 109–116. [CrossRef]
89. Hou, D.; Luo, W.; Huang, Y.; Yu, J.C.; Hu, X. Synthesis of porous $Bi_4Ti_3O_{12}$ nanofibers by electrospinning and their enhanced visible-light-driven photocatalytic properties. *Nanoscale* **2013**, *5*, 2028–2035. [CrossRef] [PubMed]
90. Villafuerte-Castrejón, M.E.; Morán, E.; Reyes-Montero, A.; Vivar-Ocampo, R.; Peña-Jiménez, J.A.; Rea-López, S.O.; Pardo, L. Towards Lead-Free Piezoceramics: Facing a Synthesis Challenge. *Materials* **2016**, *9*, 21. [CrossRef] [PubMed]
91. Bao, H.; Zhou, C.; Xue, D.; Gao, J.; Ren, X. A modified lead-free piezoelectric BZT–xBCT system with higher T_C. *J. Phys. D Appl. Phys.* **2010**, *43*, 465401. [CrossRef]
92. Zheng, T.; Wu, J.; Xiao, D.; Zhu, J.; Wang, X.; Xin, L.; Lou, X. Strong piezoelectricity in $(1-x)(K_{0.4}Na_{0.6})(Nb_{0.96}Sb_{0.04})O_{3-x}Bi_{0.5}K_{0.5}Zr_{1-y}Sn_yO_3$ lead-free binary system: Identification and role of multiphase coexistence. *ACS Appl. Mater. Interface* **2015**, *7*, 5927–5937. [CrossRef] [PubMed]
93. Zhang, S.; Yu, F. Piezoelectric Materials for High Temperature Sensors. *J. Am. Ceram. Soc.* **2011**, *94*, 3153–3170. [CrossRef]